RSC Advances

PAPER

View Article Online
View Journal | View Issue

Cite this: *RSC Adv.*, 2020, **10**, 13076

Enhanced yellow afterglow in $Ca_2SnO_4:Dy^{3+}$ by co-doping Na^+/K^+

Yue Chen, Jun Zou, * Mingming Shi and Bobo Yang

A new yellow long afterglow luminescent material $Ca_2SnO_4:Dy^{3+}$ was prepared by the solid state method at 1350 °C. The yellow LLP (long-lasting phosphorescent) material $Ca_2SnO_4:Dy^{3+}$ was prepared by co-doping alkaline ions (K^+ and Na^+) and investigated using an X-ray diffractometer (XRD), photoluminescence spectrometer, afterglow meter and thermoluminescence spectrometer. The excitation and emission spectra showed an excitation peak at 350 nm and an emission peak at 573 nm. The optimized Dy^{3+} dopant concentration was found to be 1 mol%. For the improvement in the photoluminescence performance, we can co-dope it with alkaline ions (K^+ and Na^+), with the optimal concentration of the alkaline ions being 1 mol%. On the basis of the experimental results, we constructed a probable model for explaining the mechanism of LAG in detail.

Received 21st January 2020
Accepted 11th March 2020

DOI: 10.1039/d0ra00656d

rsc.li/rsc-advances

1. Introduction

Long afterglow (LAG) luminescence is an interesting optical process with the decay time extending to seconds, minutes, or even hours after the removal of the excitation source at room temperature. As a unique luminescence phenomenon, recently, LAG has been paid a lot of attention with practical applications in various fields, for example, safety lighting, dial-up displays, decoration, storage media, high-energy ray detection, optical fiber thermometers and live biological imaging.[1–5] In this phenomenon, energy is absorbed and stored under excitation (usually ultraviolet and visible light), and emission is visible for a long period even after the excitation stops.[6–9] Because of their exceptional properties in luminescence intensity, afterglow time, and chemical stability, a lot of blue and green afterglow phosphors of silicates and aluminates have been sold in the market, while yellow long-lasting phosphors remain relatively backward.[10,11] Some reported yellow-emitting long persistent phosphors are $Sr_3SiO_5:Eu^{2+}$, Dy^{3+},[12] $Ca_2Al_2Si_2O_7:Mn^{2+}$, Ce^{3+},[13] $Sr_3Al_2O_5Cl_2:Eu^{2+}$, Tm^{3+},[14] $Ca_2ZnSi_2O_7:Eu^{2+}$, Dy^{3+},[15] $Ca_2BO_3Cl:Eu^{2+}$, Dy^{3+},[16] $Ca_6BaP_4O_{17}:Eu^{2+}$, and Ho^{3+}.[17] However, they have short persistence time and low brightness. Hence, it is urgent and very desirable to explore new types of yellow LAG.

Recently, Shi *et al.*[18] have reported a new yellow long-persistent luminescent $Ca_2SnO_4:Dy^{3+}$ whose wideband emission peak is at 573 nm, where we can observe the afterglow for several minutes in the dark after removing the excitation source. Unfortunately, the brightness and duration are not enough for practical applications. In order to use yellow LAG phosphors in practical applications, it is necessary to further enhance their initial intensity and afterglow duration.

At the same time, alkali ions (Li^+, K^+, Na^+, *etc.*) are well-known high-efficiency sensitizers, thereby enhancing the luminescence performance of the phosphors by charge compensation.[19] Therefore, we believe that some intensive studies are still needed to investigate the photoluminescence behavior and afterglow performance of the Dy^{3+} mono-doped and alkali ion (Li^+, K^+, Na^+) co-doped Ca_2SnO_4 phosphors. However, Li^+ will volatilize when heated at a temperature higher than 1310 °C, and all test reagents may transition to a glassy state, which affects the experimental results.[20] To improve the properties of the yellow afterglow phosphors, in this study, we used alkali ions (K^+ and Na^+) for the improvement in the afterglow performance of the $Ca_2SnO_4:Dy^{3+}$ phosphors. The Ca_2SnO_4 phosphors doped with Dy^{3+} and alkali metal ions (K^+ and Na^+) were obtained using the solid state reaction. We studied the luminescence properties and afterglow behavior of the phosphors. The results show that the basic ions K^+ and Na^+ can effectively improve the photoluminescence and afterglow luminescence of the phosphors.

2. Experimental

All the powder samples were prepared by a high-temperature solid-state reaction. Analytical reagents $CaCO_3$, SnO_2, Na_2CO_3, K_2CO_3, and Dy_2O_3 (99.99%) were used as raw materials. The Dy^{3+} doping concentrations were varied from 0.5 to 5 mol% and the concentration of the co-doped M^+ (M = Na, K) was adjusted from 0.2 to 1.5 mol%. In a typical process, raw materials with different stoichiometric amounts were ground together in an agate mortar for 4 h and then pressed into tablets. The tablets were heated up to 1350 °C and held at this temperature for 10 h.

School of Materials Science and Engineering, Shanghai Institute of Technology, 100 Haiquan Road, Shanghai 201418, China. E-mail: zoujun@sit.edu.cn

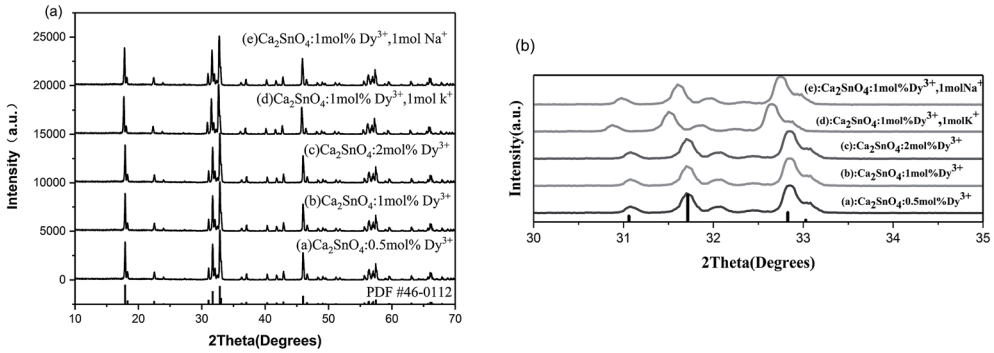

Fig. 1 XRD patterns of (a) Ca_2SnO_4:0.5 mol% Dy^{3+}, (b) Ca_2SnO_4:1 mol% Dy^{3+}, (c) Ca_2SnO_4:2 mol% Dy^{3+}, (d) Ca_2SnO_4:1 mol% Dy^{3+}, 1 mol% K^+ and (e) Ca_2SnO_4:1 mol% Dy^{3+}, 1 mol% Na^+ phosphors.

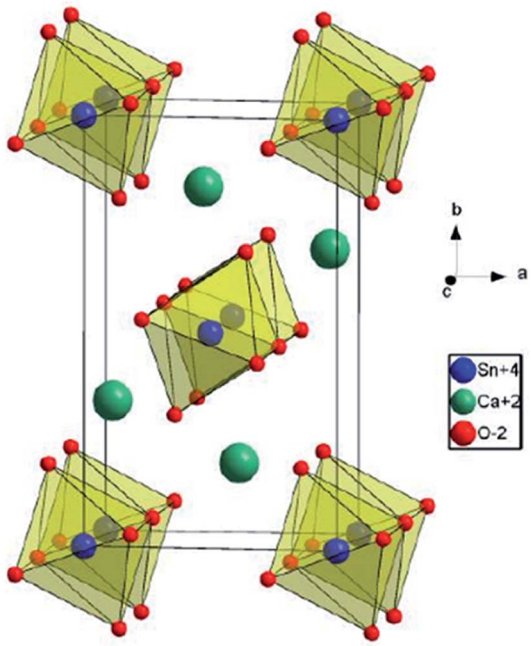

Fig. 2 The crystal structure of Ca_2SnO_4.

Then, the samples were quickly cooled to room temperature with a rate of 20 °C min^{-1}. The fired tablets were ground to obtain the phosphorous powders.

We analyzed the crystalline structure of the samples within the range of 10–70° by X-ray diffraction (XRD) with a TD3500 X-ray diffractometer (Bruker AXS, Karlsruhe, Germany). We obtained the excitation and emission spectra using Xe 900 (450 W xenon arc lamp) by an FLS-920T fluorescence spectrophotometer. The scanning step is 1 nm. We measured the thermoluminescence curve using an FJ-427-A1 thermoluminometer (Beijing Nuclear Instrument Factory) when the heating rate was 1 K s^{-1}. Before the measurement, we irradiated the sample with ultraviolet (350 nm) radiation for different time periods.

3. Results and discussions

3.1 Structural determination

X-ray diffraction (XRD) was used to detect the purity of all the prepared samples. In Fig. 1, we can see the typical XRD patterns of different concentrations of Dy^{3+} (0.5 mol%, 1 mol%, and 2 mol%) doped in Ca_2SnO_4 and Ca_2SnO_4:1 mol% Dy^{3+}, 1 mol% K^+ and Ca_2SnO_4:1 mol% Dy^{3+}, 1 mol% Na^+ phosphor samples. We have also shown the pattern for the PDF card no. 46-0112 in Fig. 1; after comparison with it, we can index all the observed peaks to the pure phase of Ca_2SnO_4. In this system, the Dy^{3+} ions were incorporated into the Ca_2SnO_4 lattice by substituting Ca^{2+} because of their similar ionic radii. All the diffraction peaks can be indexed to an orthorhombic structure according to the reference file PDF #46-0112.

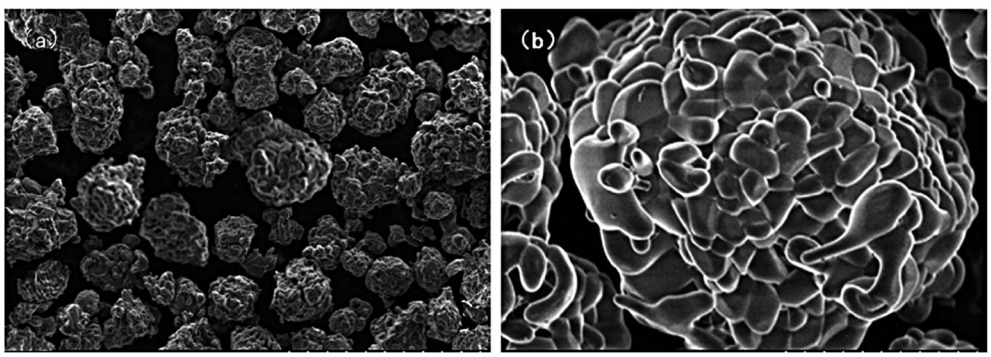

Fig. 3 SEM images of $Ca_{1.98}Dy_{0.02}SnO_4$ phosphor (a) particle uniformity and dispersion, (b) particle shape and size.

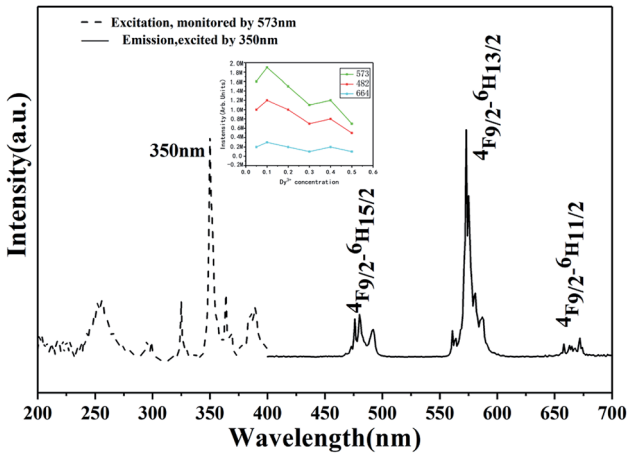

Fig. 4 Excitation (λ_{em} = 573 nm) and emission spectra (λ_{ex} = 350 nm) of Ca_2SnO_4:1 mol% Dy^{3+}phosphor.

From Fig. 1a, we can see that in Ca_2SnO_4, the mono-doping of Dy^{3+} and the co-doping of K^+ and Na^+ do not result in the formation of impurities or secondary phase. The diffraction peaks of the lattice plane, which are magnified in Fig. 1b, clearly shift towards smaller angles after doping K^+ and Na^+. Moreover, the shift in the diffraction peak is more obvious when K^+ is doped. This is expected since the larger K^+ ions replace the smaller Ca^{2+} ions in the Ca_2SnO_4 structure, consequently affecting the luminescence of the phosphors (Fig. 2).

Ca_2SnO_4 crystallizes in the orthorhombic crystal system with the space group *Pbam*; the unit cell parameters are a = 0.5753 nm, b = 0.9701 nm, and c = 0.3266 nm.[21] In the Ca_2SnO_4 crystal, the shared edges of the SnO_6 octahedron are connected into a one-dimensional chain. SnO_6 octahedron and 4 of 6 oxygens of the adjacent $2Sn^{4+}$ ions form Sn^{4+}–O^{2-} –Sn^{4+}. The other two O^{2-} ions are connected to the Sn^{4+} –O^{2-} bond at the end of Sn^{4+} ion.

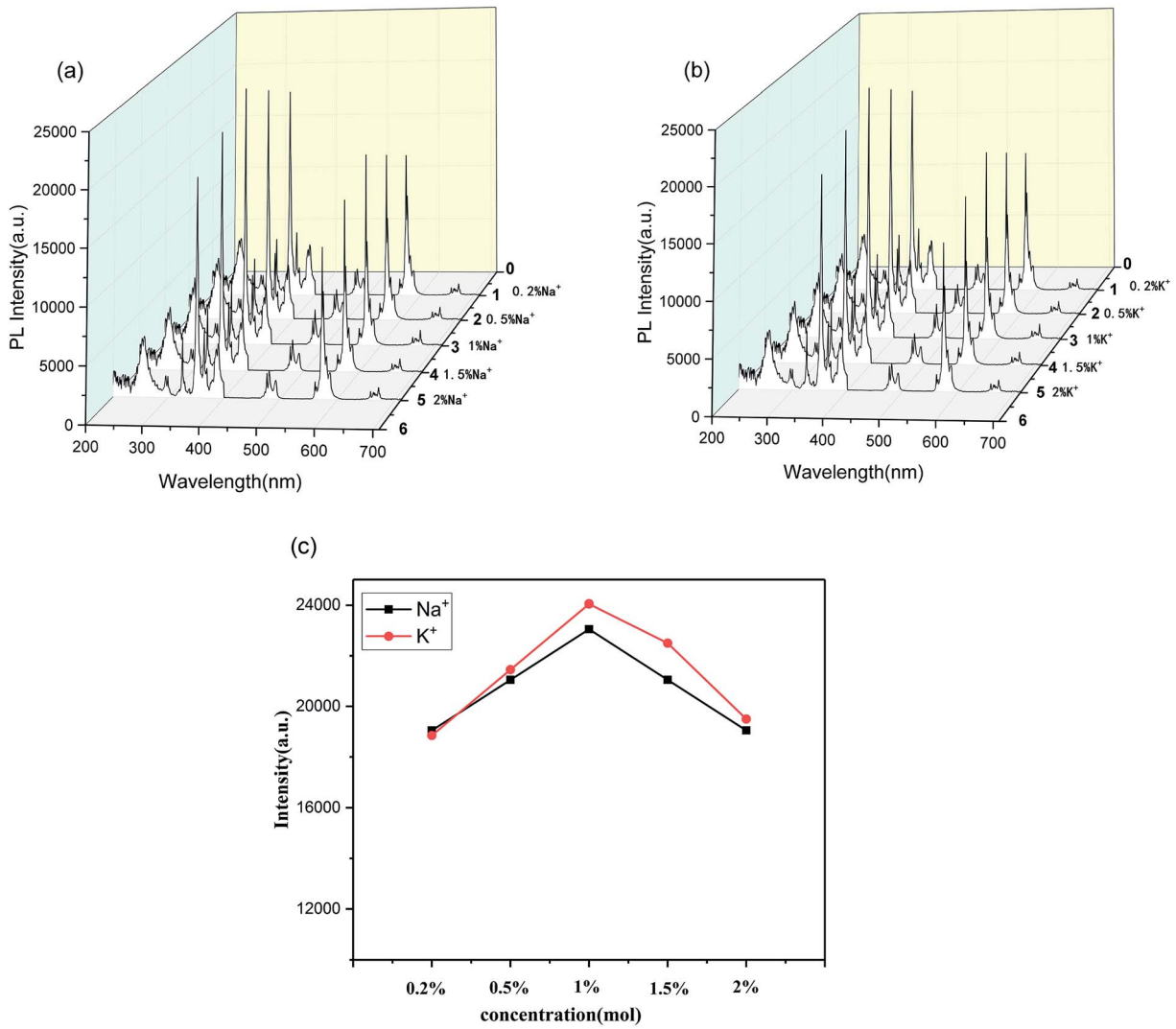

Fig. 5 PL spectra of Ca_2SnO_4:1 mol% Dy^{3+} phosphors with (a) Na^+ doping and (b) K^+ doping, and (c) the difference in K^+, Na^+ excitation intensities at different concentrations at 350 nm.

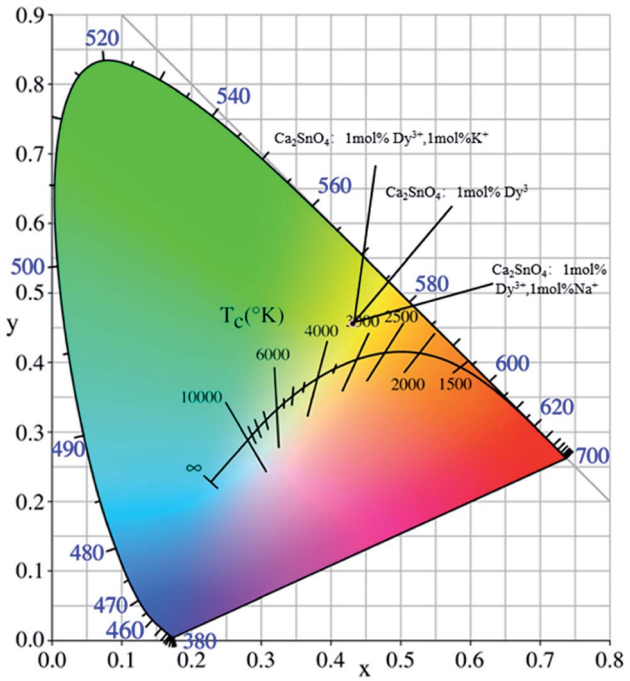

Fig. 6 The CIE 1931 chromaticity coordinates of the Ca_2SnO_4:1 mol% Dy^{3+}, Ca_2SnO_4:1 mol% Dy^{3+}, 1 mol% K^+ and Ca_2SnO_4:1 mol% Dy^{3+}, 1 mol% Na^+ phosphors.

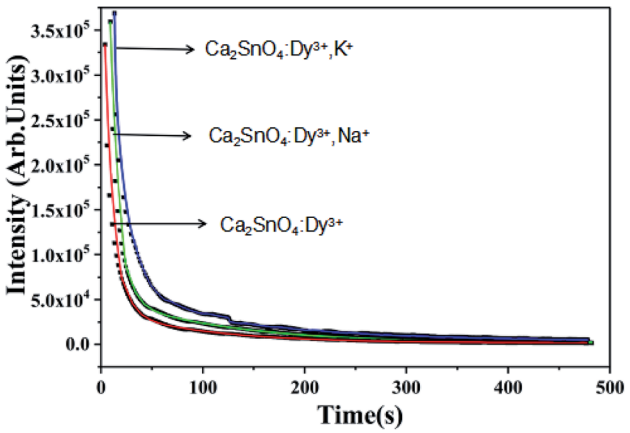

Fig. 7 Afterglow of Ca_2SnO_4:Dy^{3+}, Ca_2SnO_4:Dy^{3+}, K^+ and Ca_2SnO_4:-Dy^{3+}, Na^+ phosphors.

SEM was carried out to confirm the morphology of the $Ca_{1.98}Dy_{0.02}SnO_4$ phosphors synthesized at 1350 °C by the solid state reaction in air. The morphological images are shown in Fig. 3. It can be clearly seen from Fig. 3a that the particles are of uniform size with a good degree of dispersion. From Fig. 3b, it is clear that the prepared particles are almost spherical with a dimension in the range of 15–20 μm.

3.2 Photoluminescence characteristics

From Fig. 4, we can see the PLE as well as PL spectra of the prepared Dy^{3+}-doped Ca_2SnO_4 phosphor. There is a very strong band peak in the PLE spectrum at 350 nm because of the charge transfer of Dy^{3+}–O^{2-}. When the optimum excitation wavelength is 350 nm, there are several strong peaks in the range of 300–400 nm and 450–700 nm. They consist of the main emission and Dy^{3+} 4f–4f characteristic transition emission lines near 402 nm as well as the transition of the $^4F_{9/2}$ excited states to the $^6H_{J/2}$ ground states, covering $^4F_{9/2} \rightarrow {}^6H_{15/2}$ (482 nm), $^4F_{9/2} \rightarrow {}^6H_{13/2}$ (573 nm) and $^4F_{9/2} \rightarrow {}^6H_{11/2}$ (672 nm) separately. We can find that the intensity of the magnetic dipole transition $^4F_{9/2} \rightarrow {}^6H_{15/2}$ around 482 nm is fairly lower than that of the electric dipole transition $^4F_{9/2} \rightarrow {}^6H_{13/2}$ around 573 nm, implying that the Dy^{3+} ions occupy the positions with no inversion symmetry in Ca_2SnO_4.[22,23] This is in good agreement with the upper structural analysis results.

To further investigate how the doping of alkaline ions affects the properties of the Ca_2SnO_4:1 mol% Dy^{3+} phosphor, the excitation and emission spectra of five phosphors with various concentrations of the alkali ions were tested.[24] Fig. 5a, for the Na^+-doped phosphor, shows that the excitation and emission intensities increase as the Na^+ doping concentration increases. The intensity reaches a maximum for 1% doping and then gradually decreases. Therefore, the optimal doping concentration of sodium ions is 1 mol%. Similarly, we can also observe the results for K^+ co-doped Ca_2SnO_4:1 mol% Dy^{3+} phosphor in Fig. 5b, which shows that the excitation and emission intensities increase as the doped K^+ concentration increases; also, it is determined that the K^+ concentration is 1 mol% and the intensity is the largest.

The effect of K^+ and Na^+ doping on the PL intensity of the samples was further studied (Fig. 5c). Fig. 5c shows the difference in the excitation intensities of K^+ and Na^+ at different concentrations at 350 nm. Interestingly, the PL intensity of the Na^+-doped phosphors is lower than that of the K^+-doped phosphors, which indicates that the K^+ ions are better for the luminescence of the developed phosphors. These results largely indicate that we can dope alkali ions to improve the PL characteristics of the developed phosphor.

According to the measured emission spectra, we calculated the CIE chromaticity coordinates of different Ca_2SnO_4:1 mol% Dy^{3+}, Ca_2SnO_4:1 mol% Dy^{3+}, 1 mol% K^+ and Ca_2SnO_4:1 mol% Dy^{3+}, 1 mol% Na^+ phosphors, as shown in Fig. 6. We calculated

Table 1 Simulated results for the afterglow curves of Ca_2SnO_4:Dy^{3+}, Ca_2SnO_4:Dy^{3+}, K^+ and Ca_2SnO_4:Dy^{3+}, Na^+ phosphors

Composition	I_0	A_1	τ_1 (s)	A_2	τ_2 (s)	A_3	τ_3 (s)
Ca_2SnO_4:Dy^{3+}	959	1.4×10^7	0.8	1.2×10^6	3.9	7.9×10^4	27.0
Ca_2SnO_4:Dy^{3+}, K+	1658	1.7×10^7	0.9	1.5×10^6	4.0	9.6×10^4	27.0
Ca_2SnO_4:Dy^{3+}, Na+	1543	1.6×10^7	0.8	1.4×10^6	4.2	8.9×10^4	2.0

the CIE chromaticity coordinates as $x = 0.4535$, $y = 0.4022$. The samples co-doped with Na^+ and K^+ are also labeled in this figure. It is not difficult to see that the co-doping of Na^+ or K^+ ions has no significant effect on the color of the developed phosphor. Therefore, the as-prepared yellow phosphors have wide application prospects in w-LEDs and display applications.

3.3 Afterglow properties

We recorded the decay curves of Ca_2SnO_4:1 mol%Dy^{3+}, Ca_2SnO_4:1 mol% Dy^{3+}, 1 mol% K^+ and Ca_2SnO_4:1 mol% Dy^{3+}, Na^+ (Fig. 7) immediately after exposure to 350 nm irradiation for 5 minutes. Generally, a decay curve indicates two processes: a fast decay process and a slow decay process. We also measured the afterglow decay curve of the sample for comparison. From Fig. 7, we can see that at the beginning, the decay rate is high; then, we observe a slow decay process mainly because of the faster release rate of the charge carriers in shallow traps and the slower release rate of the charge carriers in deeper traps. It can also be seen from the figure that the initial afterglow intensity and duration of the co-doped phosphors are different from that for the rare earth element-doped phosphors. The afterglow emission and initial photoluminescence intensity of the original Ca_2SnO_4:1 mol% Dy^{3+} phosphors are lower than those of the co-doped phosphors. For a further investigation of the reason for the change in the afterglow performance, we fitted the afterglow curves of Ca_2SnO_4:1 mol% Dy^{3+}, Ca_2SnO_4:1 mol% Dy^{3+}, 1 mol% K^+ and Ca_2SnO_4:1 mol% Dy^{3+}, 1 mol% Na^+ phosphors with the following three attenuation equations:[18,25]

$$I = I_0 + \mathrm{A}_1 \exp(-t/\tau_1) + A_2 \exp(-t/\tau_2) + A_3 \exp(-t/\tau_3) \quad (1)$$

Here, I and I_0 represent the phosphorescence intensities, A_1, A_2 and A_3 represent the constants, t represents the time and τ_1, τ_2, and τ_3 represent the decay times for the three exponential components.[26] The results obtained using Origin 2017 software can be seen in Table 1. We can see the parameters from Table 1: a three index decay model represents the decay process of these phosphors, and the τ value is an important factor for the evaluation of the afterglow characteristics of the phosphors. The attenuation time τ increases as the afterglow characteristics get better. Single-doped samples have lower brightness than co-doped samples, which signifies the existence of traps. It is confirmed that co-doping with alkaline ions results in better afterglow properties.

It is also reported that the persistent time of the LAG phosphors is affected greatly by the depths, because of the slow release of the trapped charge carriers by thermal stimulation after UV irradiation, traps play an important role in the decay process.[27] Hysteresis materials that have an appropriate trap depth and large trap density usually have good properties. Hence, for the determination of the trap center, the thermally stimulated luminescence (TSL) of Dy^{3+} and alkali ion (K^+, Na^+) co-doped as well as Dy^{3+} single-doped Ca_2SnO_4 phosphors was determined, as shown in Fig. 7.

Once the phosphor is excited, electrons and holes will be produced. These electrons and holes will be captured and released step by step due to thermal disturbance. Then, light

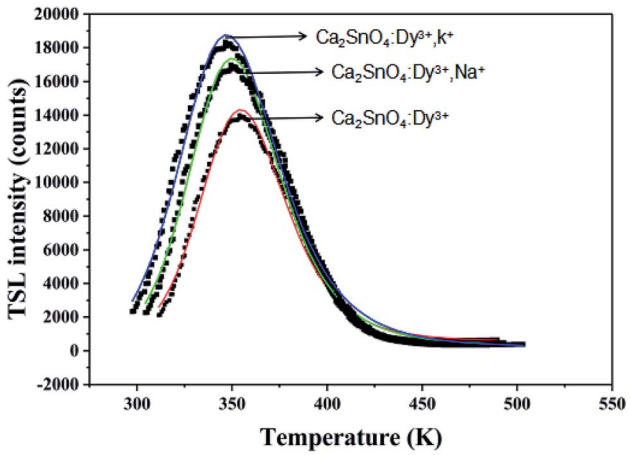

Fig. 8 TSL curves of Ca_2SnO_4:Dy^{3+}, Ca_2SnO_4:Dy^3, K^+ and Ca_2SnO_4:Dy^3, Na^+ phosphors.

Table 2 TSL parameters from the curve fitting technique

Composition	Peak temp. (K)	E_t (eV)	S	n_0
Ca_2SnO_4:Dy^{3+}	320	0.478	1682, 466	1.16×10^6
Ca_2SnO_4:Dy^{3+}, K^+	353	0.582	3140, 233	1.58×10^6
Ca_2SnO_4:Dy^{3+}, Na^+	347	0.571	1774, 536	1.47×10^6

can be emitted by the electrons and holes through radiative transitions. In general, these traps can be characterized by thermoluminescence. For the verification of the trap change, we obtained the thermoluminescence (TL) curves (Fig. 8). We can get the trap depth through the following formula:[28,29]

$$I(T) = sn_0 \exp\left(\frac{-E}{kT}\right)\left[\left(\frac{(b-1)s}{\beta}\right) \times \int_{T_0}^{\tau} \exp\left(-\frac{E}{kT'}\right)\mathrm{d}T' + 1\right]^{-\frac{b}{b-1}} \quad (2)$$

Here, I represents the intensity of the luminescence peak, s represents the frequency factor, n_0 represents the capture concentration of capture carriers, E represents the capture depth (activation energy), k represents the Boltzmann constant, β represents the heating rate (1 K s^{-1} in this paper), and b represents the kinetic order or attempt-to-escape frequency, indicating the order of the capture process: $b = 1$ for direct recombination and $b > 1$ for remapping the carriers. On the basis of the above-mentioned kinetic equation, all the thermoluminescence curves can be well-fitted by the multi-peak method. Usually, each TL peak is a capture center.[30] We can observe at least two traps of different depths. Accordingly, we can see the cutting parameters of the samples from Table 2. It can be found that such suitable trap depths were obtained with TSL peaks at low temperature (around 300–400 K). As mentioned above, the obtained phosphors have better decay performance because of the suitable capture types and capture depth.

From the fitting peaks, by using the equation $E = 25kT_m$, the trap depths related to the peaks located in the range of 350–375

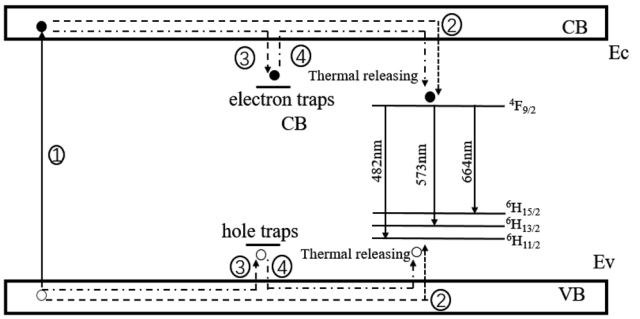

Fig. 9 A schematic graph of the phosphorescence mechanism for Ca_2SnO_4:1 mol% Dy^{3+}; ○ represent hole; ● represent electron.

K were calculated as 0.478 eV for the Ca_2SnO_4:Dy^{3+} phosphor, 0.582 eV for Ca_2SnO_4:Dy^{3+}, K^+ and 0.571 eV for Ca_2SnO_4:Dy^{3+}, Na^+.[31] Traps of appropriate depths are reported to play an important role in capturing electrons and slowly transporting them to the light-emitting center to produce afterglow.[29] If the depth of the traps is very deep, it is difficult for the trapped electrons to escape from the traps and release photons, leading to the degradation of the LLP performance.[32,33] If the trap depth is shallow, the trapped electrons can easily go back to the ground state and emit light and thus, the life of LLP is short.[32] The results show that the n_0 value increases obviously after the co-doping of K^+ and Na^+. This means that more free electrons can be trapped in more electron traps formed. Thus, we obtained brighter initial phosphorescence and a longer afterglow time. As reported before, Dy^{3+} acts as a trap supplier. In the trap, replacing Ca^{2+} will cause defects in the crystal. We can express the process as 3Ca = 2DyCa* + VCa. Two positive defects of electrons captured by DyCa* and a negative vacancy of VCa will be produced due to each substitution by two Dy^{3+} ions .[24,25] The doping of Dy^{3+} will produce deeper traps and determine the afterglow in the later stage. In addition, the introduction of basic ions M^+ (K^+, Na^+) can deepen the traps and increase the trap density, thus capturing more electrons and producing longer and stronger afterglow. We can write the equation as follows:

$$Dy^{3+} + M^+ + 2CaCa^{2+} = DyCa + MCa' + 2Ca^{2+} \quad (3)$$

Based on the experimental results, for a clearer study of the afterglow process, we can see the phosphorescence mechanism of Ca_2SnO_4:Dy^{3+} (Fig. 9) and it is described by the following key steps: (1) under UV irradiation, the electrons in the ground state of Dy^{3+} are excited to enter the conduction band (CB), due to which the holes remain in the ground state. (2) Some of the excited electrons are transferred to the excited levels of Dy^{3+} through relaxation; then, yellow photoluminescence of Dy^{3+} and the recombination of the electrons and holes occur. (3) In VB, electron traps can trap and store some excited electrons, while hole traps can capture and store holes. Therefore, part of the excitation energy is stored instead of returning to the ground state for photoluminescence.[34] (4) After UV irradiation is cut off, the electrons are released slowly from the traps under the action of thermal activation and transferred to high-energy Dy^{3+} and then, the electrons and holes combine, resulting in yellow light emission of the Dy^{3+} ions.

4. Conclusion

We obtained a yellow LLP phosphor Ca_2SnO_4:Dy^{3+} by the conventional solid state method at 1350 °C in air. XRD analysis showed that all the samples exhibited a pure phase. Under the excitation of UV light, a rare earth activator has the ability of bright self-activation and sensitization. The luminescence and afterglow properties improved by doping basic ions (K^+, Na^+). The best doping concentration of K^+ and Na^+ was 1 mol%. On this basis, a simplified hysteretic mechanism model was proposed.

Conflicts of interest

There are no conflicts to declare.

Acknowledgements

This work was supported by the National Natural Science Foundation of China (61901270), the Shanghai Sailing Program (17YF1419200) and the Science and Technology Planning Project of Zhejiang Province, China (2018C01046).

References

1 H. A. Höppe, H. Lutz, P. Morys, W. Schnick and A. Seilmeier, *J. Phys. Chem. Solids*, 2000, **61**, 2001–2006.
2 M. Kowatari, D. Koyama, Y. Satoh, K. Iinuma and S. Uchida, *Nucl. Instrum. Methods Phys. Res., Sect. A*, 2002, **480**, 431–439.
3 X. Wang, D. Jia and W. M. Yen, *J. Lumin.*, 2003, **102–103**, 34.
4 J. Chen, H. Guo, Z. Li, H. Zhang and Y. Zhuang, *Opt. Mater.*, 2010, **32**, 998.
5 Z. Pan, Y.-Y. Lu and F. Liu, *Nat. Mater.*, 2011, **11**, 58.
6 W. Zeng, Y. H. Wang, S. C. Han, W. B. Chen and G. Li, Investigation on long-persistent luminescence of Ca_2BO_3Cl:Eu^{2+}, Ln^{3+} (Ln = Nd, Dy, Er), *Opt. Mater.*, 2014, **36**, 1819–1821.
7 S. Som, S. Dutta, V. Kumar, A. Pandey, V. Kumar, A. K. Kunti, J. Priya, S. K. Sharma, J. J. Terblans and H. C. Swart, $CaTiO_3$:Eu^{3+}, a potential red long lasting phosphor: energy migration and characterization of trap level distribution, *J. Alloys Compd.*, 2015, **622**, 1068–1073.
8 J. C. Zhang, Q. S. Qin, M. H. Yu, M. J. Zhou and Y. H. Wang, The photoluminescence, afterglow and up conversion photostimulated luminescence of Eu^{3+} doped Mg_2SnO_4 phosphors, *J. Lumin.*, 2012, **13**, 23–26.
9 W. Y. Li, Y. L. Liu and P. F. Ai, Synthesis and luminescence properties of red long-lasting phosphor Y_2O_2S:Eu^{3+}, Mg^{2+}, Ti^{4+} nanoparticles, *Mater. Chem. Phys.*, 2010, **119**, 52–56.
10 B. F. Lei, B. Li, H. R. Zhang and W. L. Li, Preparation and luminescence properties of $CaSnO_3$:Sm^{3+} phosphor emitting in the reddish orange region, *Opt. Mater.*, 2007, **29**, 1491–1494.

11 B. F. Lei, B. Li, H. R. Zhang, L. M. Zhang, Y. Cong and W. L. Li, Synthesis and luminescence properties of cube-structured $CaSnO_3/RE^{3+}$(RE = Pr, Tb) long-lasting phosphors, *J. Electrochem. Soc.*, 2007, **154**, H623–H630.
12 P. Dorenbos, *J. Lumin.*, 2003, **104**, 239.
13 X.-J. Wang, D. Jia and W. M. Yen, *J. Lumin.*, 2003, **102–103**, 34.
14 Y. Li, Y. Wang, Y. Gong, X. Xu and M. Zhou, *Opt. Express*, 2010, **18**, 24853.
15 L. Jiang, S. Xiao, X. Yang, X. Zhang, X. Liu, B. Zhou and X. Jin, *Mater. Sci. Eng., B*, 2013, **178**, 123.
16 W. Zeng, Y. Wang, S. Han, W. Chen, G. Li, Y. Wang and Y. Wen, *J. Mater. Chem. C*, 2013, **1**, 3004.
17 H. Guo, W. Chen, W. Zeng, G. Li, Y. Wang, Y. Li, Y. Li and X. Ding, *J. Mater. Chem. C*, 2015, **3**, 5844.
18 M. Shi, D. Zhang and C. Chang, Dy3 :Ca_2SnO_4, a new yellow phosphor with afterglow behavior, *J. Alloys Compd.*, 2015, **639**, 168–172.
19 A. K. Bedyal, V. Kumar and H. C. Swart, Charge compensated derived enhanced red emission from $Sr_3(VO_4)_2:Eu^{3+}$ nanophosphors for white light emitting diodes and flat panel displays, *J. Alloys Compd.*, 2017, **709**, 362–372.
20 C. S. Sunandana and T. Kumaraswami, Li_4TeO_4: a new, glassy Li^+-ion conductor, *J. Non-Cryst. Solids*, 1986, **85**(1–2), 247–250.
21 R. Gupta, S. M. Kumar and F. Hussain, Syntheses, Crystal Structures and Solid-State Properties of the Lanthanoid-Containing Nanoclusters, *Eur. J. Inorg. Chem.*, 2014, **2014**(35), 6031–6038.
22 F. Shi-Liu, T. Yin and C. Fei, Synthesis and characterization of $Ca_2Sn_{1-x}Ce_xO_4$ with blue luminescence originating from Ce^{4+} charge transfer transition, *Chin. Phys.*, 2007, **16**(10), 3129–3133.
23 M. Irfanullah and K. Iftikhar, A comparative study of 1H NMR and sensitized visible light emission of an extended series of dinuclear lanthanide complexes, *J. Photochem. Photobiol., A*, 2011, **224**(1), 91–101.
24 L. Ü. Xiao, M. Sun and J. Zhang, Effect of mixing process on the luminescent properties of $SrAl_2O_4:Eu^{2+}$, Dy^{3+} long afterglow phosphors, *J. Rare Earths*, 2010, **28**(1), 150–152.
25 Y. P. Huang and J. W. Lin, The trap bag concept of afterglow luminescence, *Sci. Rep.*, 2017, **7**(1), 8475.
26 J.-Y. Bae, Reevaluation of dietary methionine requirement by plasma methionine and ammonia concentrations in surgically modified rainbow trout, Oncorhynchus mykiss, *J. Appl. Ichthyol.*, 2010, **27**(3), 887–891.
27 G. Li, Y. Wang, W. Zeng, W. Chen, S. Han, H. Guo and X. Wang, Luminescence properties of a new green afterglow phosphor $NaBaScSi_2O_7:Eu^{2+}$, *Dalton Trans.*, 2015, **44**, 17572–17578.
28 S. W. S. McKeever and R. Chen, Luminescence models, *Radiat. Meas.*, 1997, **27**, 625–661.
29 J. N. Demas, B. A. DeGraff and W. Xu, Modeling of luminescence quenching-based sensors: comparison of multisite and nonlinear gas solubility models, *Anal. Chem.*, 1995, **67**, 1377–1380.
30 Z. Zou, C. Cao and T. Zhan, Chem Inform Abstract: Structure, Long Persistent Luminescent Properties and Mechanism of a Novel Efficient Red Emitting $Ca_2Ga_2GeO_7:Pr^{3+}$ Phosphor, *Cheminform*, 2016, **47**(30), 397–405.
31 C. S. Shalgaonkar and A. V. Narlikar, Review: a review of the recent methods for determining trap depth from glow curves, *J. Mater. Sci.*, 1972, **7**, 1465e1471.
32 X. Ting, G. Hongxu, J. Zhang, C. Odetola, Y. He, H. Lin, G. Chen and Z. Zheng, Phosphorescence behavior and photoluminescence mechanism of Dy^{3+}, sensitized β-$Zn_3(PO_4)_2:Mn^{2+}$, phosphor, *J. Alloys Compd.*, 2015, **642**, 225e231.
33 Y. Li, Y. Wang, Y. Xiong, T. Peng and M. Mo, Effect of electron traps on long afterglow behavior of $Sr_3Al_2O_6:Eu_{0.01}{}^{2+}$, $Dy_{0.02-x}{}^{3+}$, $Ho_x{}^{3+}$, *J. Rare Earths*, 2012, **30**, 105e109.
34 Z. Zehua, Structure, long persistent luminescent properties and mechanism of a novel efficient red emitting $Ca_2Ga_2GeO_7:Pr^{3+}$ phosphor, *J. Alloys Compd.*, 2016, **397**.

